Experimental system for measuring the force load of a single blade pump

Dávid Bleho[1*], *Róbert Olšiak*[1], *Branislav Knížat*[1]

[1]Strojnícka Fakulta STU in Bratislava, Nám. slobody 17, 81231 Bratislava, Slovak Republic

Abstract. Precise evaluation and anticipation of the radial and axial force loads acting on the impeller of a spiral casing pump are essential to ensure that the pump operates efficiently and dependably. This study presents an experimental system for measuring the force load of a single blade pump and explores the fluid mechanics involved in its operation. The experimental system consists of a strain gauge and a data acquisition system, which measures the force load on the blade as the pump rotates. In addition, our investigation delves into various approaches for measuring radial force loads, which include the evaluation of reaction forces on bearings. For the case of experimental measurement of the radial and axial force in the pump bearings, it is necessary to make some design modifications on the pump body. The measurement methodology is based on the principle of a "relaxed" shaft that performs a so-called spherical motion around the rotation axis during pump operation.

Keywords: *Radial force; Experimental circuit; Centrifugal pump, Strain gauge*

1 Introduction

Raising the hydraulic parameters of the pumps in conjunction with an increase in impeller speed can cause the rotor or the entire machine to oscillate with excessive amplitudes, which poses a significant risk. Therefore, it is crucial to be cognizant of the rotor vibration and the cyclical stress on the bearings to ensure optimal service life. Apart from adequately dimensioning the individual parts for strength, the operating parameters of the machine, especially the overall stresses, play a critical role in determining the machine's lifespan and reliability.

As the trend towards reducing the number of impeller blades continues, a new set of challenges related to the behaviour around single blade impellers. The flow around a single blade generates significant asymmetric pressure around the impeller's circumference, leading to interactions with the pump's spiral casing that can result in strong oscillations. In the literature, this force load on the pump rotor is called hydrodynamic unbalance [1-4]. Furthermore, the pressure field varies during one impeller revolution due to the changing interaction between the impeller and the volute body [5].

* Corresponding author: david.bleho@stuba.sk

Hydrodynamic force, specifically radial force, has a significant impact on the pump shaft, resulting in radial deflections that can be observed by vibrations on the bearing blocks or in the pump body [6]. These vibrations are transmitted throughout the pump system and frequently cause pump failure or damage to the connected pipe.

2 Hydraulic loads

2.1 Axial load

Axial thrust loads in centrifugal pumps occur due to internal pressures acting on the exposed surfaces of the rotating element. The fluid in the impeller's front and rear disc spaces rotates along with the impeller, resulting in parabolic pressure patterns that vary with the impeller's radius (as illustrated in Fig. 1). This parabolic pressure distribution is a consequence of the rotating vessel theory applied to the fluid's rotational motion behind the impeller.
Several factors contribute to the axial force, such as the impeller's location relative to the stationary walls, the symmetry of the impeller discs, the wall surface roughness, the seal ring clearance, and possibly the balancing hole geometry. In recent publications, such as [7], the calculation relationship of the axial force incorporates the impact of wall roughness, side chamber dimensions, and the flow between the two sealing gaps, i.e., the front sealing ring and the gap between the shaft and the pump body. The author claims that the flow through the magnitude of the sealing gaps increases the axial force by 18% to 26%.

Since the magnitude of the angular velocity of the fluid in the space between the impeller cover disks and the pump body is assumed to be the same, that is, half the impeller speed ($\omega_{liquid} = 1/2\ \omega_{impeller}$), the pressure patterns behind the cover and carrier disks are identical. This assumption follows from the idea that the rotating impeller disk frictionally actuates the fluid in rotation and the opposite wall of the diffuser stator ‘brakes’ the fluid equally. Due to the rotation of the fluid in the side chambers, the static pressure decreases in the radial direction to the axis of the impeller. However, the pressure pattern also occurs behind the support disc at a radius smaller than the sealing gap on the rear disc. Due to the different sizes of the pressure patterns, an axial force F_a is generated.

The basic static pressure distribution and the components of the hydraulic axial thrust are shown in Fig. 1. The main part of the axial force is represented by the force components acting on the front impeller F_{fs} and the rear casing F_{bs}, which are the result of the pressure distribution on the respective surface. The smaller part represents the impulse thrust F_i resulting from the input component of the axial velocity and the resultant force due to the difference in static pressure distribution on the hub and casing streamlines F_{ch}. The force F_{ch} can reach higher values in impellers with higher specific speeds and in out-of-service conditions [8].

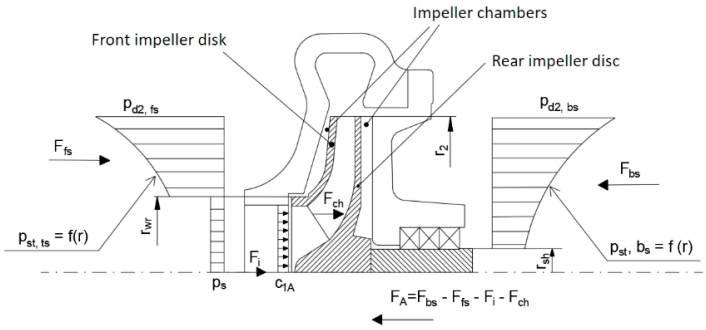

Fig. 1 Static pressure distribution for a closed impeller [8]

According to the theory of axial force calculation, the total axial thrust is larger for the case of a single-bladed semi-open impeller than for a closed impeller, and this is due to the fact that the component acting on the front part of the impeller F_{fs} is neglected here (Fig. 1). The resulting axial force calculation for semi-open impellers then takes the form:

$$F_A = F_{bs} - F_i - F_{ch} \tag{1}$$

2.2 Radial load

Radial force on the impeller results from the asymmetric pressure distribution inside the asymmetrically curved impeller blade and at the outer circumference of the impeller. The asymmetrical pressure and momentum distribution results from the geometrical shape of the pump body (spiral diffuser, bladeless, or blade diffuser), from the asymmetrical impeller inflow, or from the operating mode of the pump.

The radial force acts at a right angle to the pump shaft and is transmitted to the rotor and its bearings. This force can deflect the shaft and cause vibration due to its oscillation, ultimately leading to a system failure. Thus, determining the hydrodynamic radial force is a crucial aspect of pump design.

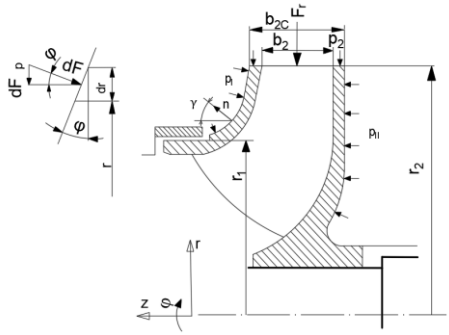

Fig. 2 Meridional section of the impeller [9]

Fig. 2 shows the silhouette of the radial impeller of the pump. For an impeller of this shape, the radial force is a result of both the compressive action on its outer surface and the hydrodynamic effect of the flowing fluid, caused by the change in its momentum. As such, the expressions for the radial force components, F_{rx} and F_{ry}, can be obtained through equations (2) and (3), respectively.

$$F_{rx} = -b_{2C}\, R_2 \int_0^{2\pi} p_2(\varphi)\, \cos(\varphi)\, \mathrm{d}\varphi =$$
$$= -\rho\, b_2\, r_2 \left(\int_0^{2\pi} c_{r2}^2(\varphi)\, \cos(\varphi)\, \mathrm{d}\varphi - \int_0^{2\pi} c_{r2}(\varphi)\, c_{u2}(\varphi)\, \sin(\varphi)\, \mathrm{d}\varphi \right) =$$
$$= -\int_0^{2\pi} \int_{r'}^{r_2} \left[p_2(\varphi) - \rho\, \frac{\omega^2}{8}\, (r_2^2 - r'^2) \right] \mathrm{tg}\, \gamma(r)\, r\, \mathrm{d}r\, \cos\varphi\, \mathrm{d}\varphi \tag{2}$$

$$F_{ry} = -b_{2C}\, r_2 \int_0^{2\pi} p_2(\varphi)\, sin(\varphi)\, d\varphi =$$
$$= -\rho\, b_2\, r_2 \left(\int_0^{2\pi} c_{r2}^2(\varphi)\, sin(\varphi)\, d\varphi + \int_0^{2\pi} c_{r2}(\varphi)\, c_{u2}(\varphi)\, cos(\varphi)\, d\varphi \right) =$$
$$= -\int_0^{2\pi} \int_{r'}^{r_2} \left[p_2(\varphi) - \rho\, \frac{\omega^2}{8}\, (r_2^2 - r'^2) \right] tg\, \gamma(r)\, r\, dr\, sin\varphi\, d\varphi \tag{3}$$

The total magnitude of the radial force is calculated as follows.

$$F_r = \sqrt{F_{rx}^2 + F_{ry}^2} \tag{4}$$

Equations (2) and (3) for the components of the radial force components, F_{rx} and F_{ry}, depend on the geometric parameters of the impeller (b_{2c}, b_2, r_2, r') which can be easily obtained by the designer. Additionally, the equations include velocity and pressure fields such as $p_2(\varphi)$, $c_{r2}(\varphi)$, $c_{u2}(\varphi)$ which need to be determined through calculation or measurement.

The magnitude of the radial force acting on a centrifugal pump is affected by a variety of factors. Alongside the structural design of the spiral and the mode of operation with respect to the Q/Q_n ratio, the impact of cavitation is also noteworthy. Specifically, the shape and design of the spiral significantly influence the course and magnitude of the radial force. Achieving a proper synchronization of the impeller and volute parts of the pump is one of the most important aspects in pump design. Ideally, if the fluid flow in the volute and at the impeller outlet was symmetrical, a constant static pressure distribution would be achieved. In practise, however, there are velocity changes in different parts of the spiral, which create a pressure differential around the circumference of the impeller and the spiral, thus generating a radial force that loads the pump rotor.

3 Structural modifications of the pump case

Since the radial force is determined in a plane perpendicular to the axis of rotation, it must be measured at least at three measuring points [10]. In our case, similar to [2] [11] [12] for more convenient measurement, up to four holes located in the plane of the front bearing (Fig. 4) are drilled and strain gauge sensors of cylindrical geometry with a 90º spacing are inserted into the holes (Fig. 4). A brass washer (Fig. 4) is inserted between the sensor body and the outer ring of the single-row ball bearing to ensure that it is centred and deflected of the bearing's protective peripheral casing. In this case, the sensitive part of the strain gauge sensor does not touch the outer ring of the bearing, but the foot of the preload screw, which is also fixed against its rotation and thus the change of the initial preload. To ensure free movement of the shaft in the radial direction, there is a clearance of approximately 1 mm between the brass washer and the body of the trestle (see Fig. 4).

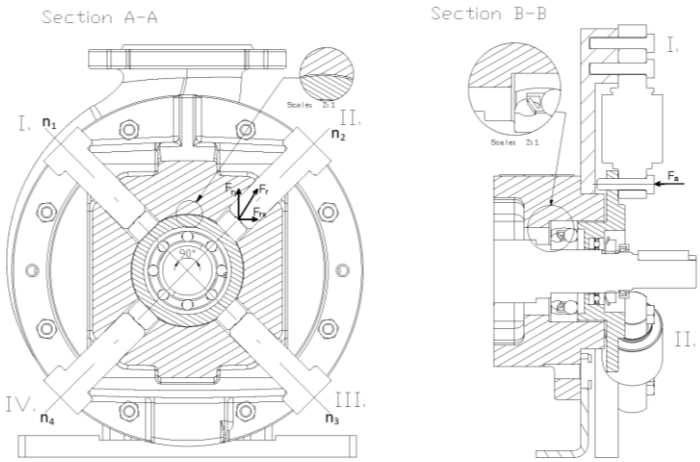

Fig. 3 Front and rear pump section showing the location of the sensors

A common approach to axial load measurement involves the use of strain gauges or load cells to directly measure the force on the rear double row bearing that is supported by the shaft. In this method, the load cells are mounted between the pump casing and the electric motor. However, this approach also requires modification of the pump and installation of additional equipment (as shown in Fig. 4 Section B-B). The sensors are attached to a non-moving base at one end, and their sensitive part is connected to the bearing housing by a rigid cylindrical body. The span between the sensors is 120 degrees so that the axial force is evaluated as the mean value at the three measurement points (Fig. 5). It is important to achieve the same preload on all three sensors in order to avoid bearing distortion or deformation of the bearing.

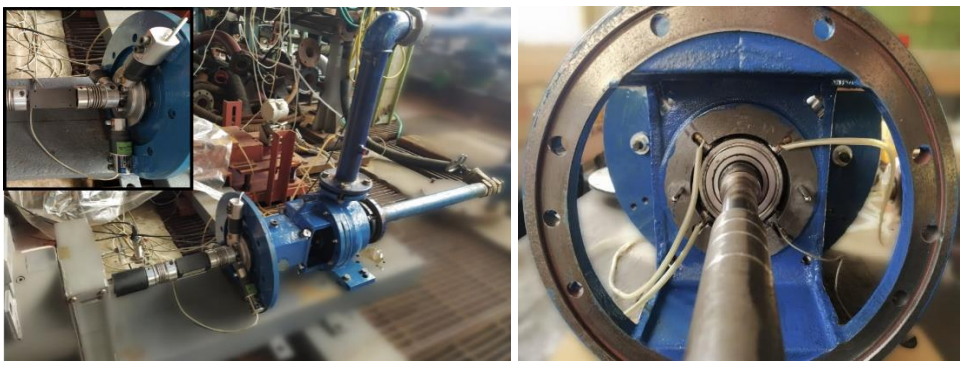

Fig. 4 Implementation of strain gauge sensors on the pump under study

4 Experimental measurement methodology

4.1 Experimental measurement circuit

Fig. 6 shows the schematic layout of the measurement system. The feed tank N_1 is designed to maintain a constant liquid level z_1 during the measurements by pumping liquid from the feed tank and returning the excess liquid via the waste collection pipe to the collection tank N_2. The supply line features a fully open shut-off valve *SV* during measurements, leading

from the pump outlet to the flow meter, continuing to the *TV* throttling valve, and ultimately terminating at the N_2 tank. The auxiliary pump *AP* is used to return the liquid from the collection tank N_2 to the supply tank N_1 to complete the test loop. The loop also comprises an evacuation system, a water-circulating pump *BP,* and a bleeding valve *BV* that is used to remove air from the system before starting the experiment, as the water level in the N_2 tank is below the axis of both the *TP* under test and the auxiliary pump *AP*.

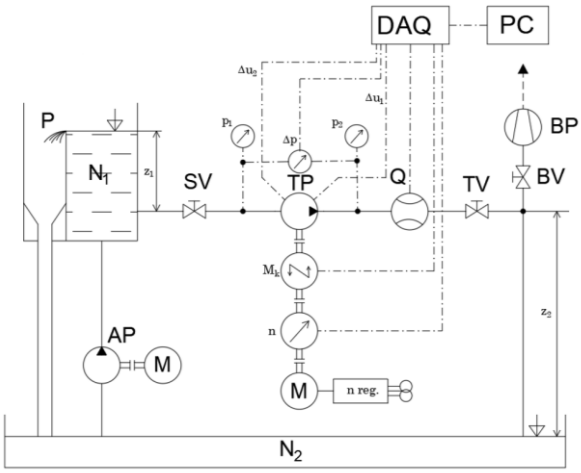

Fig. 5 Schematic of the experimental measurement circuit

To monitor the operating variables, several sensors are included in the loop. Suction side pressure p_1, discharge side pressure p_2, flow rate Q, torque M_k, and voltage change Δu, corresponding to the magnitude of the waveform of the applied forces, are monitored. All signals are processed using an analogue-to-digital converter (*DAQ*) connected to a *PC*. The *DAQ* converter is situated between two devices to establish communication and convert one physical quantity into another that can be further processed. In this case, the conversion of the nonelectrical quantity - the applied force F [N] - into an electrical quantity - the voltage U [V] is performed.

5 Principle for the evaluation of applied forces

When measuring the radial force, the forces exerted by the bearing on the sensor are determined by reading the amount of preload acquired by the preload bolt. This initial preload force $F_{0i,r}$ behaves as an action from which we subtract the mean value of the measured force response $F_{i,r}$ due to the fact that the sensor is compressive and only allows the inward force to be measured.

$$F_r = \sum_{i=1}^{i=4} F_{0i} \pm F_i \tag{5}$$

The opposite sign in the previous equation represents a situation where both forces act in the same direction or are opposite to each other.

Decomposing this into component form in the x and y axes, the following is true:

$$F_{rx,}F_{ry} = \frac{1}{\sqrt{2}} \sum_{i=1}^{i=4} F_{0i,r} \pm F_{i,r} \tag{6}$$

Then the magnitude of the resultant radial force will be of the following form:

$$|F_r| = \sqrt{F_{rx} + F_{ry}} \tag{7}$$

Determining the angle of the radial force:

$$\alpha = arctg\left(\frac{F_{ry}}{F_{rx}}\right) + \alpha_{kv} \tag{8}$$

The angle α_{kv} represents the angle of the quadrant according to Fig 4. in which the resultant radial force vector occurs.

The principle of axial force measurement is based on the displacement of the shaft due to the axial load on the impeller. A double-row bearing is pressed on the shaft, the outer sleeve of which is supported by an auxiliary flange that transmits the reaction force and connects the sensitive part of the sensor to the moving shaft. The calculation of the axial force is considerably simpler because it can act in two directions parallel to the axis of rotation of the shaft.

$$F_{ax} = F_{0,a} \pm F_{i,a} \tag{9}$$

The axial force from the preload is determined by averaging three measurement points 120º apart and will serve as an "offset".

$$F_{0,a} = \frac{1}{n}\sum_{n=1}^{3} F_{0i} \tag{10}$$

6 Results and discussion

On the basis of the experimental measurement, the radial load on the impeller was depicted in Fig. 6. All of the experiments were measured at 1450 rpm. To find the best efficiency point of the centrifugal pump, the efficiency curve was also shown. The red line on the left describes the course of the radial force magnitude, and the blue line describes the efficiency curve. It is obvious from Fig. 6 that radial force curve decreases with increasing values of the flow rate. The lowest value of the radial force is on the right side of the best efficiency point. However, the value of the radial force is never equal to zero, but from this point, with increasing flow rate, it starts to grow again.

The graph on ride side in the Fig. 6 shows direction of the radial force vector. This graph is divided into four quadrants and each quadrant represents one of the four strain gauge positions. The coordinate [0,0] represents the axis of rotation. The direction of the radial force vector was calculated according to equation (8) and its magnitude was calculated according to equation (7). As can be seen from the graph, the direction of the radial force is in all four quadrants, while the distance from the axis of rotation decreases as the magnitude of the radial force decreases. Its centre of force starts in the second quadrant and goes all the way to the first quadrant. However, it acquires the smallest distance from the axis of rotation in the fourth quadrant.

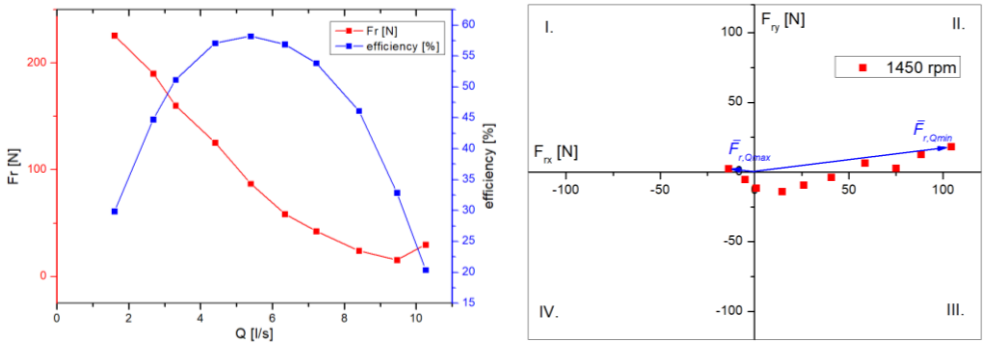

Fig. 6 Radial force magnitude and direction and efficiency curve at 1450 rpm

The individual signals obtained from the strain gauges are shown in Fig. 7. The Fig. 7 is divided into two parts, with the left side representing the time domain and the right side the frequency domain. A Fast Fourier Transformation (FFT) was used to convert between these domains.

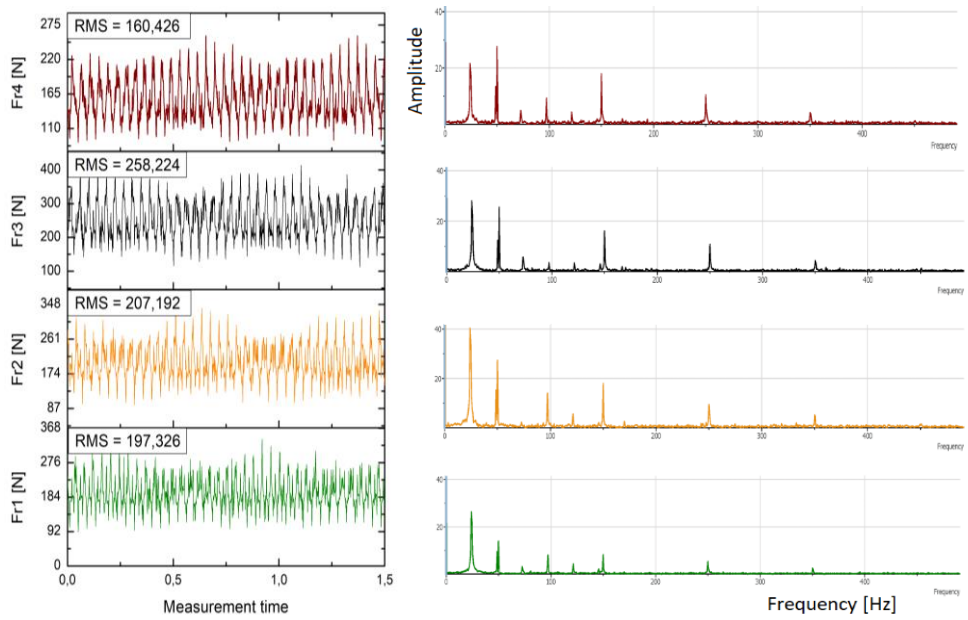

Fig. 7 Time and frequency domain of the radial force at flow 6 l/s

The Root Mean Square (RMS) statistical method was used to process the mean values of the unsteady force waveforms. RMS is the value of a set of values (or a continuous-time waveform), given as the square root of the square mean of the values or a function that is continuous (Eq. 11).

$$x_{RMS} = \sqrt{\frac{1}{n}(x_1^2 + x_2^2 + \cdots + x_n^2)} \tag{11}$$

The sampling frequency was set to 1024 Hz. The amplitudes of the main peaks appear at the rotation frequency, which is 24,1667 Hz. The pulsation frequency for the highest amplitudes, indicating the main factor of the radial force fluctuations, is the interaction between the impeller and the volute.

7 Conclusion

This article studied the behaviour of hydrodynamic forces in a centrifugal pump under different operating conditions. The radial force of the pump was investigated experimentally. Maximum values of the pressure amplitude in the impeller were observed when the pump was operated outside the design conditions.
The radial force vectors were distributed around the centre and mainly lie in 2 quadrants (II, III).

The frequency of the largest amplitude was always in steps of 24,1667 Hz, which was due to the periodic motion of the pump impeller rotation.
In the future, it is planned to compare the radial force results with CFD calculations and also measure the axial force. Overall, the results of this study may be useful for improving the design and operation of centrifugal pumps.

This article was written thanks to the generous support from the Operational Program Integrated Infrastructure for the project: “Research of physical, technical and material aspects of high-temperature reactors with the potential of hydrogen production”, project no. 313011BUH7, co-financed by the European Regional Development Fund. This work was also supported by the Slovak grant agency KEGA, project no. 016ST

References

1. Agostinelli, A.; Nobles, D.; Mockridge, C. R.: An Experimental Investigation of Radial Thrust in Centrifugal Pumps, Transactions of the ASME, Journal of Engineering for Power, Vol. 82, No. 2, 1960.
2. Okamura, T.: Radial Thrust in Centrifugal Pumps with a Single-Vane Impeller, Bull. of JSME 23, No. 180, 1980.
3. Aoki, M.: Instantanous Interblade Pressure Distributions and Fluctuating Radial Thrust in a Single-Blade Centrifugal Pump, Bulletin of the JSME 27, No. 233, 1984.
4. Gülich, J.; Jud, W.; Hughes, S. F.: Review of Parameters Influencing Hydraulic Forces on Centrifugal Impellers, Proc. Inst. Mech. Engineers, Vol. 201, No.A3, 1987.
5. Benra, F. K.; Dohmen, H. J.; Schneider, O., Unsteady Flow in Single-Blade Sewage Water Pumps, *2nd International Conference on Heat Transfer, Fluid Mechanics and Thermodynamics*, Paper No. BF1, 2003.
6. Benra, F. K., Numerical and experimental investigation on the flow induced oscillations of a single-blade pump impeller, J. *Fluids Eng*., 128(4): 783-793 (11 pages), 2006.
7. Domm, U., and Zilling, H., "Axial Thrust in Centrifugal Pumps," Preprint for the IAHR Symposium "Pumps in Power Stations," Braunschweig, 1966, pp. J23-J34.
8. Stepanoff, A. J. (1957). Centrifugal and axial flow pumps. Theory, Design, and Application.
9. Karaskiewicz, K., Szlaga, M. (2014). Experimental and numerical investigation of radial forces acting on centrifugal pump impeller. Archive of Mechanical Engineering, 445-454.
10. Tóth, P.: Vplyv interakcie rotora a statora na radiálnu silu hydrodynamického čerpadla - dizertačná práca, SjF STU Bratislava 2000.

11. Nishi, Y., J. Fukutomi, and R. Fujiwara. "Effect of blade outlet angle on radial thrust of single-blade centrifugal pump." *IOP conference series: earth and environmental science*. Vol. 15. No. 7. IOP Publishing, 2012.
12. Tan, M., et al. "Effect of Blade Wrap Angle on Performance of a Single-Channel Pump." *Experimental Techniques* 42.5 (2018): 481-490.